Interpreting attoclock experiments from the perspective of Bohmian trajectories

Wenhai Xie [1], Min Li [1,*], Yueming Zhou,[1] and Peixiang Lu[1,2]

[1]*Wuhan National Laboratory for Optoelectronics and School of Physics,*
Huazhong University of Science and Technology, Wuhan 430074, China

[2]*Hubei Key Laboratory of Optical Information and Pattern Recognition, Wuhan Institute of Technology, Wuhan 430205, China*

We theoretically study the attoclock using the Bohmian trajectory. The Bohmian trajectory includes a nonlocal quantum potential and the Coulomb potential, allowing us to separately study their effects on the attoclock. We show that the quantum potential has a significant effect on the photoelectron momentum spread while it only slightly affects the offset angle in the attoclock. We further show how the Coulomb potential affects the offset angle, revealing that the Coulomb force before the electron reaches the position of the classical tunnel exit has a significant contribution to the offset angle. Thus taking the full Coulomb effect into account during the tunneling ionization is a prerequisite for our understanding of the origin of the offset angle in the attoclock experiment. Our study also implies that there might be an inertia time for the initial wave function in response to the change of the laser electric field.

I. INTRODUCTION

Tunneling is one of the most intriguing phenomena in quantum mechanics. When an atom or a molecule is exposed to a strong laser field, the valence electron will be released by tunneling through the barrier formed by the Coulomb potential and the laser electric field. Strong-field-induced tunneling triggers a broad range of strong-field phenomena, including above-threshold ionization [1], high-harmonic generation [2,3], and nonsequential double ionization [4,5], which are basic for resolving the structure of atoms and molecules, laying the foundation of strong-field physics. Thus, a complete characterization of the strong-field-induced tunneling is important to understand those strong-field phenomena.

In elliptically or circularly polarized light fields, the instantaneous ionization time of an electron is mapped to the angle of the final momentum in the polarization plane. Thus attosecond-resolved electron dynamics can be investigated from the photoelectron angular distribution using the mapping relation [6–9]. This technique, dubbed attoclock, has been widely used to study the strong-field-induced tunneling. For instance, the attoclock has been employed to measure the tunneling time [6,10–14] to determine the position of the tunnel exit [15] and the nonadiabaticity of the tunneling process [16,17], and to reconstruct the electron subbarrier phase [18]. In the attoclock, an offset angle in the final momentum distribution was actively discussed in the past decade [10,11,13,14,19–21]. Up to now, whether the offset angle is related to the tunneling time is still under controversy.

In most previous studies, the attoclock is often interpreted based on classical or semiclassical models [10,15,19,22–24]. In those models, the classical trajectories start to propagate from the position of the tunnel exit. After tunneling, the electron motion in the combined laser and Coulomb fields is governed by the Newtonian equation. The experimental results are compared with the calculated results by the classical models to identify the possible tunneling time. Alternatively, the current of the wave function combined with classical trajectories after the tunnel exit has also been used to study the attoclock [11,25–32]. Some different tunneling properties have been found by using this combined model, e.g., it is found that the tunneling time and initial longitudinal velocity are nonzero using the classical tunnel exit as the tunneling criteria. Due to the quantum nature of tunneling ionization, the obtained conclusion of finite tunneling time or not might be incorrect based on those classical models. Bohmian mechanics is a candidate to investigate the attoclock which overcomes the above difficulty. In principle, Bohmian mechanics is equivalent to quantum mechanics, thus it is very accurate [33–36]. More importantly, Bohmian mechanics relates the wave function dynamics to the particle trajectories, i.e., Bohmian trajectories [37,38]. Compared with the classical trajectory, the Bohmian trajectory includes the effect of a nonlocal quantum potential and follows the current of the probability density. The Bohmian trajectory has been used to study the interaction of atoms with intense laser pulses, showing that the quantum potential becomes negligible after the electron leaves the atomic core [39,40]. Recently, the Bohmian trajectory has further been used to explore the subcycle multiphoton ionization dynamics [35,37,41] and the tunneling process [34,36], but it has not been used to study the attoclock.

In this paper, we employ Bohmian trajectories to explore the tunneling property in the attoclock. We find that Bohmian trajectories deviate from the classical trajectories beyond the tunnel exit due to the effect of the quantum potential. We show that the quantum potential has a significant effect on

*mli@hust.edu.cn

the electron trajectory even after the classical tunnel exit. We also find that the offset angle of the attoclock is rarely affected by the quantum potential after the tunneling, which is mainly influenced by the Coulomb effect near the classical tunnel exit. Using the classical tunnel exit as the tunneling criteria, we show that there is a nonvanishing time delay between the maximum ionization rate and the peak of the electric field for Bohmian trajectories. This time delay might be partially contributed by an inertia time of the initial wave function in response to the variation of the laser electric field.

This paper is organized as follows: In Sec. II, the theoretical methods are described. In Sec. III, we present our main results. The influence of the quantum potential and Coulomb potential on the final photoelectron momentum distribution (PMD) is discussed. Finally, we give a brief summary of the paper in Sec. IV. Atomic units are used throughout unless specified otherwise.

II. THEORETICAL APPROACH

A. Time-dependent Schrödinger equation

To investigate the ionization of atoms in a few-cycle circularly polarized field, we numerically solve the two-dimensional time-dependent Schrödinger equation (TDSE) of a H atom. In the length gauge, the TDSE reads

$$i\frac{\partial}{\partial t}\psi(\mathbf{r}, t) = \left[-\frac{\nabla^2}{2} + V(\mathbf{r}) + \mathbf{r} \cdot \mathbf{E}(t)\right]\psi(\mathbf{r}, t). \quad (1)$$

The Coulomb interaction between the electron and the proton was approximated by a soft-core potential $V(\mathbf{r}) = -1/(r^2 + a^2)^{1/2}$. We set the soft-core parameter as $a = 0.798$ to match the ionization potential of the H atom. The laser electric field $\mathbf{E}(t)$ is related to the vector potential $\mathbf{A}(t)$ by

$$\mathbf{E}(t) = -\frac{\partial \mathbf{A}(t)}{\partial t}. \quad (2)$$

The vector potential is given by

$$\mathbf{A}(t) = A_0 \sin^4(\omega t/2n)[\cos(\omega t)\mathbf{e}_x - \sin(\omega t)\mathbf{e}_y]. \quad (3)$$

Here ω is the frequency of an 800-nm field. The pulse length is parametrized with the number of optical cycles n and $\mathbf{A}$ vanishes for $|t - t_c| > nT/2$, where $t_c = nT/2$ corresponds to the pulse center and $T = 2\pi/\omega$ is laser field period. In the simulations throughout the article, we use a two-cycle ($n = 2$) circularly polarized laser pulse.

The split-operator spectral method [42] on a Cartesian grid is used to numerically solve the two-dimensional TDSE. The Cartesian grid ranges from -400 to 400 a.u. for both directions with a grid size of $\Delta x = \Delta y = 0.195$ a.u. The initial wave function is prepared by imaginary-time propagation [43]. In our simulation, the time step of the propagation is $\Delta t = 0.055$ a.u. For each 100 time steps, we split the electron wave function into two parts,

$$\psi(\mathbf{r}, \tau_i) = M_s(r, R_b)\psi(\mathbf{r}, \tau_i) + [1 - M_s(r, R_b)]\psi(\mathbf{r}, \tau_i)$$
$$= \psi_{\text{inner}}(\mathbf{r}, \tau_i) + \psi_{\text{outer}}(\mathbf{r}, \tau_i), \quad (4)$$

where $M_s(r, R_b) = 1 - 1/(1 + e^{-(r-R_b)/\Delta})$ is the absorption function [44] that separates the propagation space into the inner and outer regions smoothly. In the present simulation,

we choose $R_b = 150$ a.u. and $\Delta = 8.0$ a.u. The wave function in the inner region is propagated under the full Hamiltonian numerically, while in the outer region, the wave function is projected to momentum space,

$$C(\mathbf{p}, \tau_i) = \int \frac{e^{-i[\mathbf{p}+\mathbf{A}(\tau_i)]\cdot\mathbf{r}}}{2\pi} \psi_{\text{outer}}(\mathbf{r}, \tau_i)d^2r. \quad (5)$$

Then we propagate $C(\mathbf{p}, \tau_i)$ to the end of the pulse using the Volkov propagator [45],

$$C^f(\mathbf{p}, \tau_i) = e^{-i\int_{\tau_i}^{t_f} \frac{1}{2}[\mathbf{p}+\mathbf{A}(t)]^2 dt} C(\mathbf{p}, \tau_i). \quad (6)$$

Finally, we obtain the PMD by the relation

$$\frac{dP(\mathbf{p})}{dEd\theta} = \left|\sum_{\tau_i} C^f(\mathbf{p}, \tau_i)\right|^2. \quad (7)$$

Here, $E = p^2/2$ is the electron energy and θ is the angle of the emitted electron. At the end of the pulse, the wave function is further propagated for an additional four optical cycles to ensure that all the ionized components move away from the core.

B. Bohmian trajectories

In quantum mechanics, the wave function is described by the TDSE, i.e., Eq. (1). The wave function is complex and can be expressed as $\psi(\mathbf{r}, t) = R(\mathbf{r}, t)\exp[iS(\mathbf{r}, t)]$, where R and S are real. Then we obtain

$$\frac{\partial S}{\partial t} + \frac{(\nabla S)^2}{2} + V_c(\mathbf{r}, t) - \frac{1}{2}\frac{\nabla^2 R}{R} = 0, \quad (8)$$

$$\frac{\partial \rho}{\partial t} + \nabla \cdot (\rho \nabla S) = 0. \quad (9)$$

Here $\rho = R^2$ is the probability density and $\mathbf{j} = \rho \nabla S$ can be regarded as the current of the probability density. In Bohmian mechanics [33], the wave function is replaced by an ensemble of particles. Equation (9) is the continuity equation for a current probability density and describes the conservation of the probability of the ensemble, and Eq. (8) is the Hamilton-Jacobi equation for the particles. One can see that each particle trajectory is affected by a classical potential $V_c = V(\mathbf{r}) + \mathbf{r} \cdot \mathbf{E}(t)$ and a nonlocal quantum potential $V_Q = -\frac{1}{2}\frac{\nabla^2 R}{R}$.

In the simulation process, we solve the TDSE, i.e., Eq. (1), to obtain the time-dependent wave function. As the wave function $\psi(\mathbf{r}, t)$ evolves with time, the Bohmian trajectories are propagated by solving the equation of motion

$$\frac{d\mathbf{r}_j(t)}{dt} = \mathbf{v}(\mathbf{r}_j(t), t). \quad (10)$$

Here j is the index of each Bohmian trajectory. The velocity of the particle in Eq. (10) is given by

$$\mathbf{v} = \nabla S = \text{Im}\frac{\nabla \psi}{\psi}, \quad (11)$$

in the length gauge. Note that the expression of the velocity depends on the gauge choice. In Eq. (11), the time-dependent wave function ψ obtained by solving the TDSE [Eq. (1)], instead of S obtained by solving Eqs. (8) and (9), was used. We solve Eq. (10) using the fourth-order Runge-Kutta scheme.
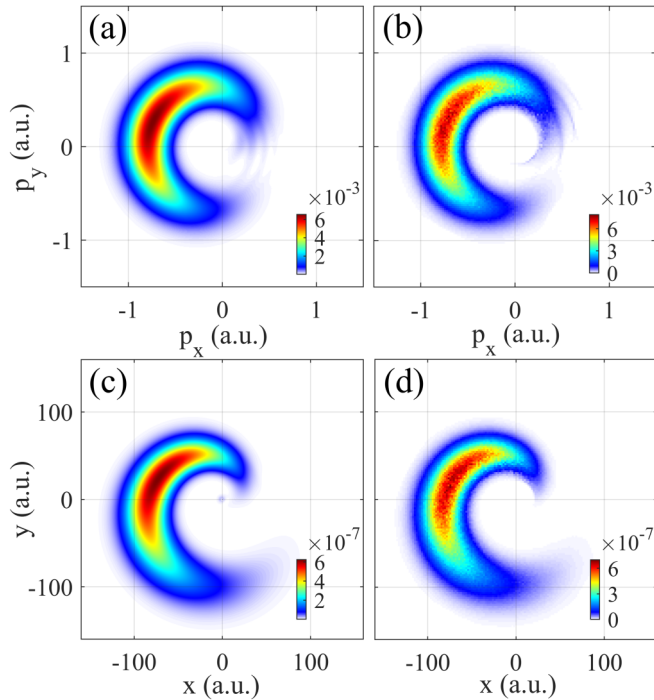
FIG. 1. (a), (b) The PMDs and (c), (d) the wave function probability distributions at the end of the laser pulse at the laser intensity $I = 1.0 \times 10^{14}$ W/cm^2. Panels (a) and (c) are the TDSE results and panels (b) and (d) are obtained from the Bohmian trajectory. The side lengths of the bins are (b) 0.02 a.u. and (d) 2 a.u.

The wave function at every other step of its propagation is used to evaluate the velocities of the trajectories at the midpoint of one Runge-Kutta step to achieve the fourth-order accuracy. In the current work, 16 million trajectories are launched with the initial positions sampled as one random variable in the position interval $[-10, 10] \times [-10, 10]$. Each Bohmian trajectory is weighted by $w_j = ds|\psi(r_j, t = 0)|^2$, where ds is the area occupied by each trajectory on average. At the limit of $ds \to 0$, the weight w_j assigned at the initial time is conserved over the time evolution [46]. Since the ionized wave packet is far from the core and does not reach the absorption boundary at time $t = 2.5T$, we define the ionized trajectories as those trajectories satisfying $r_j(t = 2.5T) > R_m$. The value of R_m is not important, as long as the value of this parameter exceeds atomic dimensions. We use $R_m = 20$ a.u. in the present work. In the following, we only concentrate on those ionized Bohmian trajectories. Finally, we obtain each point in the momentum distribution by collecting a large number of Bohmian trajectories with a momentum belonging to a square-shaped bin in the momentum plane at time $t = 2.5T$ and dividing the sum by the bin area.

III. RESULTS AND DISCUSSION

Figures 1(a) and 1(b) show the PMDs calculated by the TDSE and Bohmian trajectory at the laser intensity $I = 1.0 \times 10^{14}$ W/cm^2. The PMD from the Bohmian trajectory is nearly the same as that of TDSE, and their offset angles between the peaks of the PMDs relative to the $-x$ direction are

identical. In Figs. 1(c) and 1(d), we show the wave function probability distributions at the end of the pulse. Note that the ground state has been projected out of the wave function. One can see that the ionized wave function probability distributions are also identical for the TDSE and Bohmian mechanics. For the TDSE, the PMD shown in Fig. 1(a) can be viewed as the asymptotic photoelectron momentum obtained by the Fourier transformation of the ionized part of the wave function shown in Fig. 1(c). It appears that the velocity of the Bohmian trajectory is a local momentum, while the velocity obtained by Fourier transformation is a nonlocal momentum. Actually, in Bohmian mechanics, the velocity is not fully local, since the Bohmian trajectories are not independent of each other but linked by the nonlocal quantum potential [33].

The Bohmian mechanics is a trajectory-based method, allowing us to separately study the individual effect of the Coulomb potential and the quantum potential on the final result. We first explore the influence of quantum potential on the PMD. The Bohmian trajectories are acted by the classical force and quantum force during the propagation. When the quantum force approaches zero, the Bohmian trajectories become classical trajectories. To reveal how the quantum potential affects the PMD, we separate the whole coordinate space into two regions by setting a circle with a radius of r_i, as shown in Fig. 2(a). r_i is referred to as the transition position in the following text. In the inner region, $r < r_i$, the trajectories are influenced by both classical and quantum forces, i.e., they are Bohmian trajectories. The inner region can be called the quantum region. When those trajectories get out of the inner region, i.e., $r > r_i$, the quantum force turns off. The Bohmian trajectories become classical trajectories obeying the Newtonian equation. The outer region is called the classical region. In the outer region, the classical trajectories are obtained by numerically solving the classical Newtonian equation, i.e., $\ddot{\mathbf{r}} = -\mathbf{r}/r^3 - \mathbf{E}(t)$, starting from the transition position. Figure 2(a) shows a typical trajectory. One can see that the classical trajectory deviates significantly from the Bohmian trajectory due to the neglect of the quantum potential.

Figures 2(b)–2(e) show the PMDs with different r_i. When the transition position r_i is close to the classical tunnel exit, which is ≈ 12 a.u. for the laser parameter used here, the radial distribution of the PMD is narrow, as shown in Fig. 2(b). With the increase of r_i, the width of the radial distribution increases, as also shown in Fig. 3(b). When the transition position r_i is as large as 30 a.u., the PMD approaches the result of the fully quantum model, as shown in Figs. 1(b) and 2(e). In the previous studies, some classical or semiclassical models, such as classical-trajectory Monte Carlo [10,15,47] and quantum-trajectory Monte Carlo [48], are used to study the PMD, in which it is usually assumed that the electron has an initial transverse velocity distribution at the exit of the tunnel. The initial velocity distribution at the tunnel exit is directly related to the radial distribution of the PMD. Here, using the Bohmian trajectory, we show that the radial distribution originates from the effect of the quantum force on the electron trajectory after the tunnel exit.

To analyze how the quantum force affects the radial distribution of the attoclock, we calculate the quantum force at
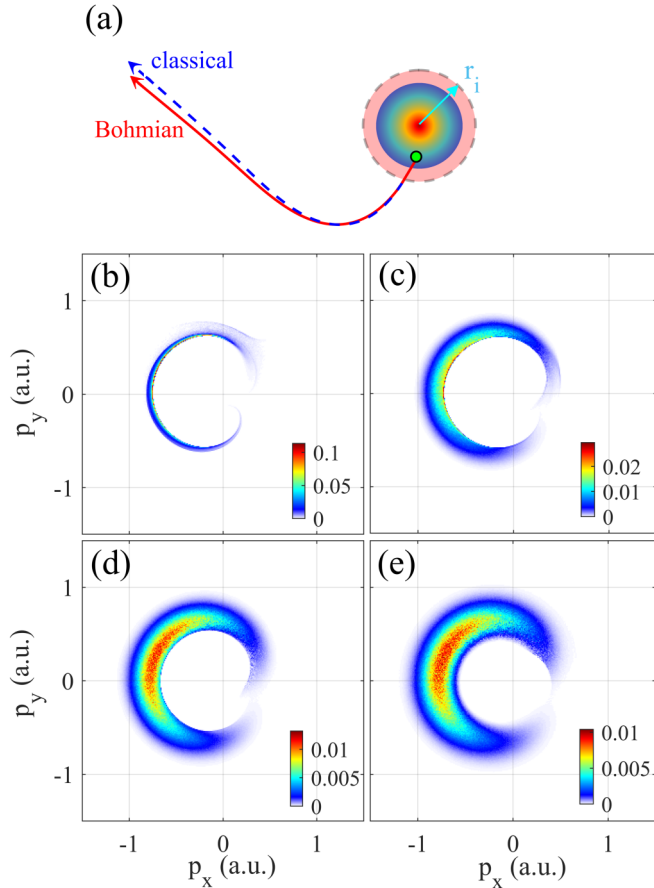
FIG. 2. (a) Starting from the initial position (green dot), the Bohmian trajectory (red curve) reaches a transition circle with a radius r_i (gray dash circle). Outside the transition circle, the quantum force is neglected and the trajectory becomes classical (blue dash curve). The classical trajectory will deviate from the original Bohmian trajectory because the quantum force is neglected. (b)–(e) The asymptotic momentum distributions using the Bohmian trajectories with different transition positions. The transition positions of the Bohmian trajectories are (b) 10 a.u., (c) 15 a.u., (d) 20 a.u., and (e) 30 a.u. The side lengths of the bins are 0.01 a.u.

different r_i and average the quantum force $\mathbf{F}_Q = -\nabla V_Q$ over the trajectories as

$$\overline{F}_Q = \frac{\sum_j w_j F_{Qj}(r_i)}{\sum_j w_j}. \tag{12}$$

The result is shown in Fig. 3(c). One can see that the average quantum force decreases with the increase of the distance r_i. Because of the quantum force, the trajectories are not classical near and even after the exit of tunnel. When the electron-core distance becomes larger, the quantum force approaches zero and the trajectories become classical. The quantum force acted on the electron after the tunnel exit position causes the radial spread of the final PMD, as shown in Figs. 2(b)–2(e). To see more clearly how the quantum force causes the radial spread of the final PMD, we calculate the quantum force along the trajectories corresponding to different points in the final PMD in Figs. 1(b). In Fig. 3(d), we show the quantum force as a function of the transition position for three points in the PMD,
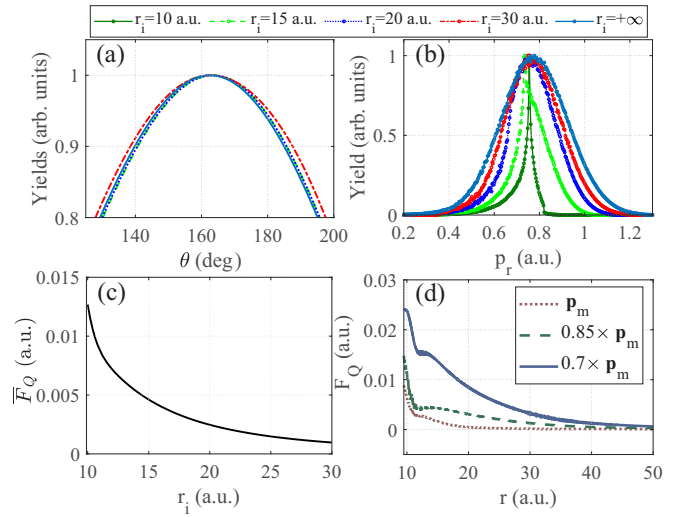

FIG. 3. The (a) angular and (b) radial distribution of the asymptotic momentum distributions for different transition positions. (c) The averaged quantum force of the Bohmian trajectories as a function of the transition position. (d) The quantum force along the Bohmian trajectories with different asymptotic momenta.

i.e., $\mathbf{p}_m$, $0.85\mathbf{p}_m$, and $0.7\mathbf{p}_m$, in which $\mathbf{p}_m$ corresponds to the maximum of the PMD. For the maximum $\mathbf{p}_m$ of the PMD, the quantum force approaches zero quickly, while for the cases of $0.85\mathbf{p}_m$ and $0.7\mathbf{p}_m$, the quantum force along the trajectories reveals a long tail. The long tail of the quantum force causes the radial spread of the final PMD. This means that the quantum potential has a significant effect on the electron trajectory even after the classical tunnel exit.

Next, we use the Bohmian trajectory to explore the origin of the offset angle in the attoclock of a H atom. We note that the angular shift of the PMD in an elliptically polarized laser field has also been called Coulomb asymmetry [49,50]. Disentangling the influence of the Coulomb field from the Coulomb asymmetry remains a key issue to understand the dynamics of the strong-field ionization. We first study the influence of quantum force on the offset angle of the PMD after the tunnel exit. We show in Fig. 3(a) the angular distribution of the PMDs with different r_i. One can see that the offset angles of the maximum of the PMD with respect to the $-x$ direction are nearly the same ($\approx 17.5°$). Therefore, the offset angle is not related to the quantum force after the tunnel exit. We then investigate the influence of Coulomb force on the offset angle in the PMD. For this purpose, we employ a similar model used in Fig. 2 but ignore both Coulomb force and quantum force at the classical region ($r > r_i$). We calculate the offset angle of the final momentum with respect to the $-x$ direction as a function of r_i, as shown in Fig. 4. We can see that the offset angle increases with increasing r_i. The offset angle changes rapidly with respect to r_i near the classical tunnel exit, as shown by the open circle, which means that the offset angle is mainly contributed by the Coulomb force near the tunnel exit. Here the classical tunnel exit is obtained by using the Landau's effective potential theory [51]. Using the tunnel exit obtained from nonadiabatic tunneling model [30] would not change the above result.
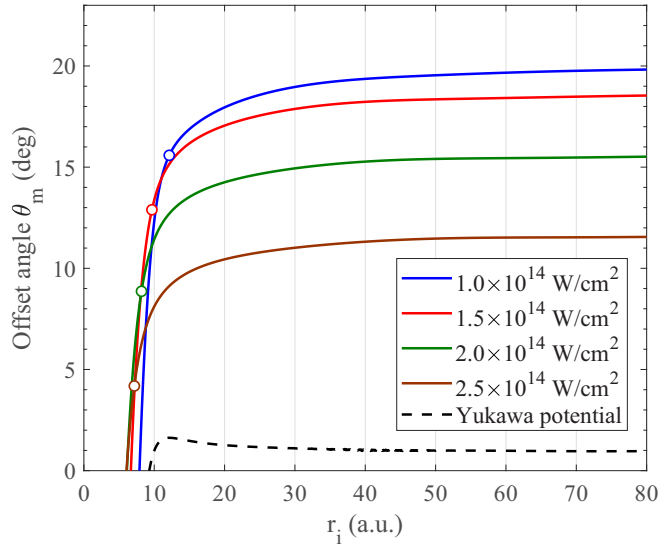
FIG. 4. The offset angle of the asymptotic momentum with respect to the transition position r_i for different laser intensities. Here both quantum potential and Coulomb potential are ignored for the outer classical region. The open circles indicate the classical tunnel exit calculated by the Landau's effective potential theory.
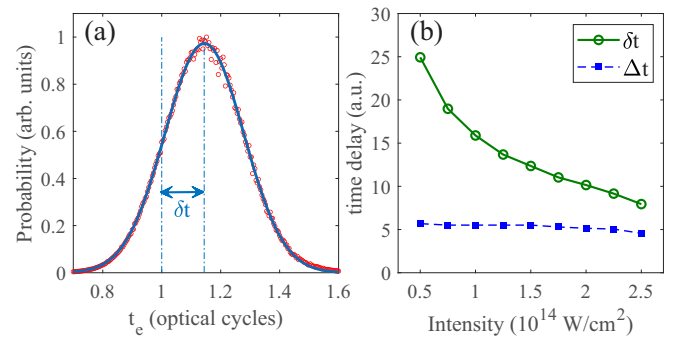

FIG. 5. (a) The distribution of the arrival time at the classical tunnel exit calculated by the Bohmian trajectories. The solid line is the Gaussian fitting curve. The time delay between the Gaussian distribution peak and the laser-field peak is indicated by δt. (b) The time delay of the arrival time (green line) and the inertia time (blue line) as a function of the laser intensity. See text for details.

We also show in Fig. 4 the offset angle as a function of r_i for different laser intensities. The final offset angles decrease with increasing the laser intensity. For all laser intensities, the offset angle changes rapidly as a function of r_i near the classical tunnel exit. One can also see, before the Bohmian trajectory reaches the tunnel exit position, the action of the Coulomb force has led to part of the offset angle for the final momentum. Thus the Coulomb force before the classical tunnel exit has a non-negligible contribution to the offset angle in the attoclock experiment [52]. The dashed line in Fig. 4 represents the offset angle in the short-range Yukawa potential, $V(\mathbf{r}) = -Ze^{-r/a_s}/(r^2 + b^2)^{1/2}$, with $Z = 2.05$, $a_s = 2$, and $b = 1.2$ for matching the ionization potential of the H atom. Compared with previous studies [13,14], the screening parameter of a_s is chosen to be 2 a.u. to ensure a comparably large ionization probability. In this short-range potential, the Coulomb tail is almost completely screened, and the quantum force does not affect the offset angle. Consequently, the offset angle in the short-range potential is close to zero.

The Bohmian trajectories represent the flux of the probability. They begin at the initial positions in the box $[-10, 10] \times [-10, 10]$, instead of the exit position used in the classical models [10,15,48]. In previous works [25,26], it has been shown that the arrival time for the maximum of the flux at the tunnel exit is after the laser electric-field peak using the virtual detector approach. Here, we also study the arrival time t_e of the Bohmian trajectories at the position of the classical tunnel exit. The arrival time distribution is shown in Fig. 5(a). The open circles are the calculated results and the solid line is the Gaussian fitting curve. One can clearly see a time delay between the peak of the electric field and the peak of the arrival time distribution at the tunnel exit. We note that in Refs. [25,26] the whole current including

the ionized and the nonionized parts is considered using the virtual-detector approach while here we only concentrate on the ionized part. The whole current $\mathbf{j} = \rho\mathbf{v}$ is also related to the probability density of the ground state, which will contaminate the observed time delay of the ionized wave function. In comparison, the arrival time distribution in Fig. 5(a) is derived from the postselected final Bohmian trajectories, corresponding to the weak measurement value for the exit time [32,38]. For the short-range Yukawa potential, there is still a large exit time delay between the arrival time peak and the instant of the laser electric-field peak even though the offset angle of the PMD is near zero. In Fig. 5(b), we show the time delay δt between the arrival time peak and the instant of the laser electric-field peak with respect to the laser intensity. One can see that the time delay decreases with increasing the laser intensity.

In the Bohmian mechanics, we can link any part of the time-dependent wave function to the initial wave function at $t = 0$ by the Bohmian trajectories. Thus, we can see the initial position distribution of the ionized wave packet in the attoclock, as shown in Fig. 6. The initial position of the ionized wave packet surrounds the center of the initial wave function. Since the peak of the electric field (along the $+y$ direction) corresponds to the highest ionization rate, the angular distribution of the initial position should peak in the $-y$ direction. Surprisingly, the angular distribution of the initial position does not peak at the reverse direction of the peak electric field. Rather, there is a deflection angle ϕ for the peak of the angular distribution of the initial position relative to the $-y$ axis.

The origin of the deflection angle shown in Fig. 6 could probably be understood as a result of the intrinsic inertia for the wave function in response to the change of the electric field in quantum mechanics. Previously, the Mandelstam-Tamm time has been defined to investigate the wave function inertia for a system with a time-independent Hamiltonian, i.e., the inability to adopt instantaneously to a field [26]. Here, the inertia time of the initial wave function in the strong field might be intuitively related to the deflection angle in Fig. 6 by $\Delta t = \phi/\omega$. In Fig. 5(b), the blue dashed line with squares
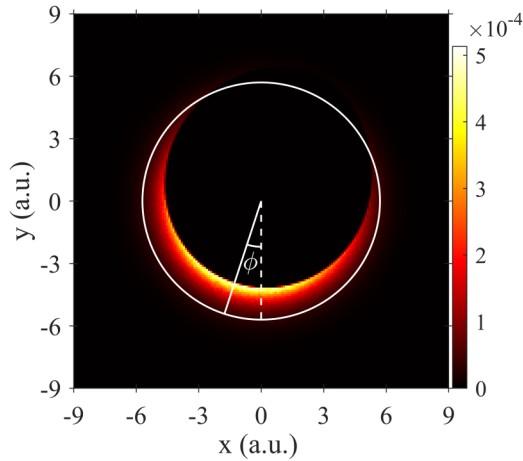
FIG. 6. The initial position distribution of the ionized Bohmian trajectories at the laser intensity $I = 1.0 \times 10^{14}$ W/cm^2. There is a deflection angle ϕ between the maximum of the initial position distribution (solid line) with respect to the maximum field direction (white dashed line). The white circle centered on the origin is used to guide the eyes.

shows the inertia time with respect to the laser intensity. One can see that the inertia time of the initial wave function is almost 100 as for the H atom and it does not change with the laser intensity.

IV. CONCLUSION

In summary, we have explored the attoclock with the Bohmian trajectories. By turning off the quantum force of the Bohmian trajectories, we found that the spread of the radial distribution of the final PMD results from the effect of the quantum force after the classical tunnel exit, which means that the trajectory after the classical tunnel exit cannot be simply considered to be classical. Furthermore, we ruled out the influence of the quantum force after the classical tunnel exit on the offset angle of the final PMD. We show that the offset angle is mainly determined by the Coulomb effect near the position of the classical tunnel exit. We also find a deflection angle between the direction of the maximum of the initial wave function distribution for the ionized Bohmian trajectories and the direction of the electric-field peak. This deflection angle might be relevant to the inertia time of the initial wave function in response to the change of the laser electric field.

[1] P. Agostini, F. Fabre, G. Mainfray, G. Petite, and N. K. Rahman, Phys. Rev. Lett. **42**, 1127 (1979).

[2] P. B. Corkum, Phys. Rev. Lett. **71**, 1994 (1993).

[3] D. Shafir, H. Soifer, B. D. Bruner, M. Dagan, Y. Mairesse, S. Patchkovskii, M. Y. Ivanov, O. Smirnova, and N. Dudovich, Nature (London) **485**, 343 (2012).

[4] D. N. Fittinghoff, P. R. Bolton, B. Chang, and K. C. Kulander, Phys. Rev. Lett. **69**, 2642 (1992).

[5] B. Walker, B. Sheehy, L. F. DiMauro, P. Agostini, K. J. Schafer, and K. C. Kulander, Phys. Rev. Lett. **73**, 1227 (1994).

[6] P. Eckle, A. N. Pfeiffer, C. Cirelli, A. Staudte, R. Dörner, H. G. Muller, M. Büttiker, and U. Keller, Science **322**, 1525 (2008).

[7] J. Yan, W. Xie, M. Li, K. Liu, S. Luo, C. Cao, K. Guo, W. Cao, P. Lan, Q. Zhang, Y. Zhou, and P. Lu, Phys. Rev. A **102**, 013117 (2020).

[8] W. Quan, V. V. Serov, M. Wei, M. Zhao, Y. Zhou, Y. Wang, X. Lai, A. S. Kheifets, and X. Liu, Phys. Rev. Lett. **123**, 223204 (2019).

[9] A. Staudte, S. Patchkovskii, D. Pavičić, H. Akagi, O. Smirnova, D. Zeidler, M. Meckel, D. M. Villeneuve, R. Dörner, M. Y. Ivanov, and P. B. Corkum, Phys. Rev. Lett. **102**, 033004 (2009).

[10] A. S. Landsman, M. Weger, J. Maurer, R. Boge, A. Ludwig, S. Heuser, C. Cirelli, L. Gallmann, and U. Keller, Optica **1**, 343 (2014).

[11] N. Camus, E. Yakaboylu, L. Fechner, M. Klaiber, M. Laux, Y. Mi, K. Z. Hatsagortsyan, T. Pfeifer, C. H. Keitel, and R. Moshammer, Phys. Rev. Lett. **119**, 023201 (2017).

[12] E. Yakaboylu, M. Klaiber, and K. Z. Hatsagortsyan, Phys. Rev. A **90**, 012116 (2014).

[13] L. Torlina *et al.*, Nat. Phys. **11**, 503 (2015).

[14] U. Sainadh, H. Xu, X. Wang, A. Atia-Tul-Noor, W. Wallace, N. Douguet, A. Bray, I. Ivanov, K. Bartschat, A. Kheifets, R. Sang, and I. Litvinyuk, Nature (London) **568**, 75 (2019).

[15] A. N. Pfeiffer, C. Cirelli, M. Smolarski, D. Dimitrovski, M. Abu-samha, L. B. Madsen, and U. Keller, Nat. Phys. **8**, 76 (2012).

[16] A. N. Pfeiffer, C. Cirelli, A. S. Landsman, M. Smolarski, D. Dimitrovski, L. B. Madsen, and U. Keller, Phys. Rev. Lett. **109**, 083002 (2012).

[17] K. Liu, S. Luo, M. Li, Y. Li, Y. Feng, B. Du, Y. Zhou, P. Lu, and I. Barth, Phys. Rev. Lett. **122**, 053202 (2019); S. Luo, M. Li, W. Xie, K. Liu, Y. Feng, B. Du, Y. Zhou, and P. Lu, Phys. Rev. A **99**, 053422 (2019).

[18] M. Han, P. Ge, J. Wang, Z. Guo, Y. Fang, X. Ma, X. Yu, Y. Deng, H. J. Wörner, Q. Gong, and Y. Liu, Nat. Photon. **15**, 765 (2021).

[19] A. W. Bray, S. Eckart, and A. S. Kheifets, Phys. Rev. Lett. **121**, 123201 (2018).

[20] V. V. Serov, A. W. Bray, and A. S. Kheifets, Phys. Rev. A **99**, 063428 (2019).

[21] V. V. Serov, J. Cesca, and A. S. Kheifets, Phys. Rev. A **103**, 023110 (2021).

[22] M. Klaiber, K. Z. Hatsagortsyan, and C. H. Keitel, Phys. Rev. Lett. **114**, 083001 (2015).

[23] A. S. Kheifets, J. Phys. B: At. Mol. Opt. Phys. **53**, 072001 (2020).

[24] C. Hofmann, A. S. Landsman, and U. Keller, J. Mod. Opt. **66**, 1052 (2019).

[25] N. Teeny, C. H. Keitel, and H. Bauke, Phys. Rev. A **94**, 022104 (2016).

[26] N. Teeny, E. Yakaboylu, H. Bauke, and C. H. Keitel, Phys. Rev. Lett. **116**, 063003 (2016).

[27] X. Wang, J. Tian, and J. H. Eberly, Phys. Rev. Lett. **110**, 243001 (2013).

[28] H. Ni, U. Saalmann, and J. M. Rost, Phys. Rev. Lett. **117**, 023002 (2016).

[29] H. Ni, U. Saalmann, and J. M. Rost, Phys. Rev. A **97**, 013426 (2018).

[30] H. Ni, N. Eicke, C. Ruiz, J. Cai, F. Oppermann, N. I. Shvetsov-Shilovski, and L. W. Pi, Phys. Rev. A **98**, 013411 (2018).

[31] M. Han, P. Ge, Y. Fang, X. Yu, Z. Guo, X. Ma, Y. Deng, Q. Gong, and Y. Liu, Phys. Rev. Lett. **123**, 073201 (2019).

[32] T. Zimmermann, S. Mishra, B. R. Doran, D. F. Gordon, and A. S. Landsman, Phys. Rev. Lett. **116**, 233603 (2016).

[33] D. Bohm, Phys. Rev. **85**, 166 (1952); **85**, 180 (1952).

[34] N. Douguet and K. Bartschat, Phys. Rev. A **97**, 013402 (2018).

[35] N. Takemoto and A. Becker, J. Chem. Phys. **134**, 074309 (2011).

[36] I. A. Ivanov, C. H. Nam, and K. T. Kim, Sci. Rep. **7**, 39919 (2017).

[37] P. Botheron and B. Pons, Phys. Rev. A **82**, 021404(R) (2010).

[38] S. Kocsis, B. Braverman, S. Ravets, M. J. Stevens, R. P. Mirin, L. K. Shalm, and A. M. Steinberg, Science **332**, 1170 (2011).

[39] X. Y. Lai, Q. Y. Cai, and M. S. Zhan, Eur. Phys. J. D **53**, 393 (2009).

[40] X. Y. Lai, Q.-Y. Cai, and M. S. Zhan, New J. Phys. **11**, 113035 (2009).

[41] H. Z. Jooya, D. A. Telnov, P.-C. Li, and S.-I. Chu, Phys. Rev. A **91**, 063412 (2015).

[42] M. D. Feit, J. A. Fleck, Jr., and A. Steiger, J. Comput. Phys. **47**, 412 (1982).

[43] M. Protopapas, C. H. Keitel, and P. L. Knight, Rep. Prog. Phys. **60**, 389 (1997).

[44] S. Chelkowski, C. Foisy, and A. D. Bandrauk, Phys. Rev. A **57**, 1176 (1998).

[45] X. M. Tong, K. Hino, and N. Toshima, Phys. Rev. A **74**, 031405(R) (2006).

[46] S. Garashchuk and V. A. Rassolov, J. Chem. Phys. **118**, 2482 (2003).

[47] J. Liu, Y. Fu, W. Chen, Z. Lü, J. Zhao, J. Yuan, and Z. Zhao, J. Phys. B: At. Mol. Opt. Phys. **50**, 055602 (2017).

[48] M. Li, J.-W. Geng, H. Liu, Y. Deng, C. Wu, L.-Y. Peng, Q. Gong, and Y. Liu, Phys. Rev. Lett. **112**, 113002 (2014).

[49] G. G. Paulus, F. Zacher, H. Walther, A. Lohr, W. Becker, and M. Kleber, Phys. Rev. Lett. **80**, 484 (1998).

[50] S. P. Goreslavski, G. G. Paulus, S. V. Popruzhenko, and N. I. Shvetsov-Shilovski, Phys. Rev. Lett. **93**, 233002 (2004).

[51] L. D. Landau and E. M. Lifschitz, *Quantum Mechanics (Non-relativistic Theory)* (Oxford University Press, New York, 1958).

[52] C. Wang, X. Li, X. Liu, J. Li, S. Zhou, Y. Yang, X. Song, J. Chen, W. Yang, and D. Ding, arXiv:2104.06144.